JOURNAL OF PROPULSION AND POWER
Vol. 15, No. 2, March–April 1999

Modeling of Stationary Plasma Thruster-100 Thruster Plumes and Implications for Satellite Design

David Y. Oh* and Daniel E. Hastings†
Massachusetts Institute of Technology, Cambridge, Massachusetts 02139
and
Colleen M. Marrese,‡ James M. Haas,‡ and Alec D. Gallimore§
University of Michigan, Ann Arbor, Michigan 48109

A computational model of a stationary plasma thruster (SPT) has been developed using a quasineutral particle-in-cell/direct simulation Monte Carlo (PIC–DSMC) model. This model is based on theoretical work showing that the plume consists of a quasineutral plasma with collisionless electrons in which the magnetic field can be neglected. Details of the PIC–DSMC method are presented as well as axisymmetric and three-dimensional results. Comparisons are made to new and previously reported experimental data. The model is shown to produce results similar to laboratory measurements of the ion current density and plume-induced sputter erosion rates. The model does not compare as well with retarding potential analyzer measurements of the ion energy distribution. The results confirm previous observations that measurements made in some ground facilities may substantially overpredict the amount of backflow current that will be experienced under operational conditions. A surface-sputtering model is used to predict the impact the plume has on solar array interconnects and to show the impact an SPT thruster could have on a communications satellite. The results show that the thruster should be canted with respect to the solar array, lowering its effective thrust and specific impulse.

Nomenclature

A = anode exit area
a_0 = local speed of sound
$\bar{c}_e$ = mean electron thermal velocity
c_r = relative speed between collision partners
E = ion impact energy, eV
$\dot{E}$ = electric field
E_d = drift energy, eV
E_r, E_z = components of electric field
e = elementary charge, 1.6×10^{-19} C
F = total thrust
f = ion distribution function
j = ion current density, mA/cm^2
k = Boltzmann's constant, 1.38×10^{-23} J/K
$\ell n\, \Lambda$ = Spitzer logarithm
m = satellite mass
$\dot{m}$ = mass flow rate
$\bar{m}_{i/e}$ = ion/electron mass
n = generic number density
n_e = electron number density
n_{ref} = reference electron number density
n_0 = neutral number density
P = pressure
r = radial position
S = sputtering coefficient, atoms/atom
T_e = electron temperature
T_i = axial ion temperature
t = thruster operation time
v = ion velocity
$\boldsymbol{v}$ = velocity vector
v_b = beam velocity
$v_\perp$ = velocity perpendicular to magnetic field
w = width of anode exit
Z_i = ionization state
z = axial distance from Anode exit
α = flow divergence angle
β = cumulative probability function
Γ_i = ion flux
Δv = change in velocity
ε = ion energy
ε_0 = permittivity of free space, 8.854×10^{-12} F/m
θ = azimuthal angle
η_i = ionization fraction
λ_d = Debye length
λ_{ee} = electron–electron mean free path
λ_{ei} = electron–ion mean free path
λ_{en} = electron–neutral mean free path
ρ_{ge} = electron gyro radius
ρ_{gi} = ion gyro radius
σ = collision cross section
φ = electrical potential
χ = particle scattering angle

Introduction

AT the present time, satellites use chemical propulsion systems for stationkeeping and other applications. When compared with chemical thrusters, electric propulsion offers the potential for substantial mass savings. While a typical bipropellant chemical thruster has a specific impulse of 320 s, Hall and ion thrusters achieve specific impulses in excess of 1500 s. One system that has shown particular promise is the stationary plasma thruster (SPT). This device has a near-optimum specific impulse for north–south (N–S) stationkeeping and is currently being marketed for use on Western satellites. Although SPT thrusters have an extensive Soviet flight heritage, Western designers have expressed concern that the plasma plumes emitted by SPTs may erode and contaminate

Received Aug. 11, 1997, revision received July 25, 1998; accepted for publication July 13, 1998.

*Research Assistant, Department of Aeronautics and Astronautics, 77 Massachusetts Avenue.
†Professor, Department of Aeronautics and Astronautics, 77 Massachusetts Avenue. Fellow AIAA.
‡Research Assistant, Department of Aeronautics and Astronautics.
§Associate Professor, Department of Aeronautics and Astronautics. Member AIAA.

sensitive satellite surfaces. These concerns must be addressed before SPTs can be used on satellites.

Substantial experimental work has been conducted to study SPT plume contamination issues, and ion fluxes, ion distributions, plume-induced sputtering and contamination have all been studied in ground-based experiments.[1-5] However, relatively little effort has been made to model processes occurring in the plume region. Existing models are empirical, relatively simple, and not well suited to modeling realistic geometries.[6-8] Detailed theoretical models are needed to fully characterize the plume region and to model the interaction between the plume and the surfaces of a satellite.

A computational model of the plume from an SPT thruster has been developed using a combination of the particle-in-cell (PIC) and direct simulation Monte Carlo (DSMC) methods to model charge exchange (CEX) collisions and to track ions and neutrals in the plume. The plume model has been combined with a surface-interaction model to estimate sputtering damage on surfaces exposed to the plume. Axisymmetric and three-dimensional versions of the code have been developed and are shown to produce qualitative agreement with multiple sources of experimental data. The model runs on workstation-class machines and should be useful to designers interested in evaluating the impact of SPT thrusters on a satellite.

This paper describes the PIC–DSMC method and presents a series of comparisons between the axisymmetric model and experimental data. Comparisons are made to measurements of the ion current density, the ion energy distribution, and surface erosion rates in the plume. Axisymmetric results showing the operation of the SPT-100 thruster in conditions that cannot be duplicated on the ground are presented and several observations are made about the plume region. Three-dimensional results are presented showing an SPT thruster mounted on a generic geostationary communications satellite. The impact of the thruster on solar array interconnects is studied and the implications for thruster placement and thruster duty cycle are discussed. These results emphasize modeling of the SPT-100 thruster because this is the most extensively studied Hall thruster at this time. In principle, the simulation can be modified and applied to new Hall and anode layer (TAL) thrusters as additional data become available.

Basic Theory and Fundamental Parameters

The SPT-100 thruster has been studied extensively and its basic characteristics are well documented. This section reviews these characteristics and derives fundamental plume parameters. The calculations are approximate, but justify assumptions made in the computational model. The following text lists the basic characteristics of the SPT-100 thruster: inner anode diameter[1] = 56 mm, outer anode diameter[1] = 100 mm, cathode orifice diameter[9] = 0.5 mm, propellant = Xe, propellant flow rate[2] = 5.2 mg/s, fraction of propellant directed to cathode[2] = ~10%, electron temperature[3] at z = 2–4 m = 2–3 eV, axial ion velocity[1] = ~17,000 m/s, fraction of ions that are double ions[1] ~20%, and ionization fraction[2] >95%. The plume's density can be estimated from the previous list, based on simple assumptions. The approximate plasma and neutral densities at the exit are given by flux conservation:

$$n_e = \eta_i \dot{m}/v_b A, \qquad n_0 = (1 - \eta_i)\dot{m}/a_0 A \tag{1}$$

Substituting from the SPT-100 list gives exit densities of n_e = 2.4×10^{17} m^{-3} and n_0 = 9.3×10^{17} m^{-3}. The plasma and neutral density in the far field can be estimated by assuming that the density falls as $(w/z)^2$. The resulting plasma densities are shown in Table 1 and are of the same order as existing experimental data.[3] Experimental measurements of the neutral density are not presently available.

A variety of fundamental parameters can be estimated from the ion and neutral density. Table 1 lists many of these parameters. The methods used to obtain these values are discussed next.

Table 1 Estimates of fundamental plasma parameters in plume

Plume parameter	Axial distance from thruster exit plane: 0.2 m	1.0 m
n_e	2.7×10^{15} m^{-3}	1.1×10^{14} m^{-3}
n_o	6.9×10^{15} m^{-3}	2.8×10^{14} m^{-3}
λ_d	0.02 cm	0.10 cm
ρ_{ge}	5.4 cm	540 cm
ρ_{gi}	230 m	>20,000 m
λ_{en}	908 m	22,700 m
λ_{ee}	26 m	660 m
λ_{ei}	35 m	880 m

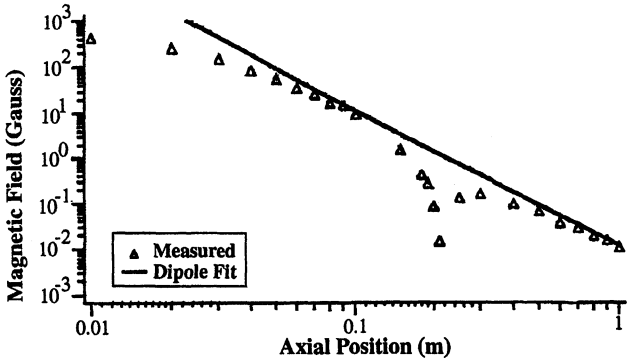

Fig. 1 Experimental measurements of the magnetic field in the plume.

Debye Length

The characteristic length over which a charge is neutralized in a plasma is the Debye length.[10] The Debye lengths shown in Table 1 are based on an electron temperature of 2 eV. In general, λ_d is small with respect to features of interest in the plume region. Even 4 m from the thruster exit, λ_d is only 0.55 cm. The plume is therefore quasineutral, except in a thin sheath region near solid surfaces. The observation that the plume is quasineutral is used to simplify the PIC portion of the model (as discussed in the next section).

Gyro Radius

A magnetic field is present in an SPT's acceleration channel to capture electrons and encourage impact ionization of the Xe propellant. The extent to which this magnetic field *leaks* into the plume region has been measured experimentally and is shown in Fig. 1.[¶] The importance of the magnetic fields in the plume region is measured by the gyro radii:

$$\rho_{gi/e} = m_{i/e} v_\perp / eB$$

The plume ion gyro radii given in Table 1 are very large and show that the ions are essentially unmagnetized; i.e., their trajectories are unaffected by the presence of the magnetic field. In addition, although the electrons are strongly magnetized inside the discharge chamber, the electron gyro radius is quite large 20 cm from the thruster and very large 1 m away. The results indicate that the influence of the magnetic field on electrons can be ignored at distances >25 cm from the thruster exit. In addition, experimental work suggests that plume characteristics are only indirectly affected by the magnetic field.[4] The ion distribution appears to be determined well inside the thruster, and small variations in the strength of the magnetic field were observed to have little influence on the plume struc-

[¶]Randolph, T., private communication, Space Systems Loral, Internal Memorandum.

ture. We therefore neglect the magnetic field throughout the plume region.

Mean Free Path

The importance of collisions is measured by the mean free path, which is given by

$$\lambda = 1/(n\sigma) \tag{2}$$

In an SPT plume, electrons can collide with three different species: ions, neutrals, and other electrons. Each species has its own collision cross section and mean free path. The total electron–Xe (neutral) collision cross section has been determined experimentally. For electrons with an average energy of 2 eV, the cross section is $\sim 1.6 \times 10^{-19}$ m^2.[11] The resulting electron neutral mean free path is given in Table 1. These values are large with respect to the plume, so that if the electrons are unmagnetized, electron–neutral collisions can be neglected.

The electron–electron and electron–ion collision cross sections are based on coulombic interactions and can be calculated from theory. Banks gives the average electron–ion cross section for $T_e/m_e \gg T_i/m_i$.[12] The result, in cgs units, is

$$\bar{\sigma}_{ei} = \frac{\pi}{2} \frac{(Z_i e^2)^2 \ell n \Lambda}{(kT_e)^2}$$

The resulting λ_{ei} (calculated with $T_e = 2$ eV) is also extremely large with respect to features of interest.

The mean self-collision cross section for singly ionized species is given by[13]

$$\bar{\sigma}_{ee} \cong (5.85 \times 10^{-10}) \ell n \Lambda / T_e^2 \text{ m}^2$$

For an electron temperature of 2 eV, this gives $\sigma = 1.4 \times 10^{-17}$ m^2, which results in the λ_{ee} values listed in Table 1. These values are also much larger than features of interest in the plume. Therefore, in the absence of a magnetic field, electrons are effectively collisionless in the plume region.

In summary, the following assumptions can be made about the plume of an SPT-100 thruster.

1) The Debye length is small, and so the plume is quasineutral, except near surfaces.
2) The ions are unmagnetized.
3) The electrons are unmagnetized.
4) The electrons are collisionless.

Computational Method

Axisymmetric Model

The PIC–DSMC method uses macroparticles to model gases at a molecular level. The algorithm is a combination of the PIC and DSMC methods described by Birdsall and Langdon[14] and Bird,[15] respectively. Because these methods are well known individually, only features specific to the SPT model are described.

The plume simulation moves ion and neutral macroparticles by integrating the equations of motion using the leapfrog method. In axisymmetric coordinates, the equations of motion for unmagnetized, collisionless ions are

$$\ddot{r} + r\dot{\theta}^2 = qE_r/m_i \tag{3a}$$

$$r\ddot{\theta} + 2\dot{r}\dot{\theta} = 0 \tag{3b}$$

$$\ddot{z} = qE_z/m_i \tag{3c}$$

The electric field is determined by differentiating the potential. In conventional PIC schemes, the potential is obtained by solving Poisson's equation. In a quasineutral plasma, however, the potential can be obtained by inverting the electron momentum equation. For collisionless, unmagnetized electrons, the momentum equation is

$$m_e n_e (\boldsymbol{v} \cdot \nabla)\boldsymbol{v} = en_e \dot{E} - \nabla p$$

At low drift velocities, the first (inertial) term can be neglected. An isothermal assumption is consistent with existing experimental data, and so the result is the familiar Boltzmann relationship[3]:

$$n_e = n_{\text{ref}} \exp(e\phi/kT_e) \tag{4}$$

Experimental measurements of the electron temperature in the plume indicate that the electrons are roughly isothermal with an electron temperature between 2 and 3 eV.[3] Based on this data, an electron temperature of 2 eV is assumed in the plume model. Simulation conducted at other electron temperatures show that small variations (± 1 eV) have little effect on the results. The potential can therefore be obtained as follows. The ion density is determined by weighting macroparticles to the nodes of an embedded grid. Particles are weighted using the cylindrical weighting functions given by Ruyten.[16] Because the plume is quasineutral, the electron density is set equal to the ion density, and Eq. (4) is inverted to obtain the potential. The result is a fast method free of many of the restrictions present with conventional PIC codes. Because the plasma is quasineutral by assumption, the Debye length does not limit the size of the grid cells. Grid cell sizes are limited by geometry and the need to resolve potential gradients. Similarly, time steps are limited by energy conservation and the need to ensure that particles move a small distance relative to the width of local potential gradients. In practice, we ensure that the fastest beam ions in the simulation move about one grid cell in each time step.

Collisional processes are modeled between move steps using the DSMC method. The variation used in this work is the multispecies local time counter method described by Elgin,[17] a variation of the DSMC algorithm described by Bird.[15] A selection–rejection scheme is used to choose collision pairs, and a single local time counter is used to determine the collision frequency for all collision processes. The collision processes included in the PIC–DSMC model are as follows: charge exchange = Xe–Xe$^+$ and Xe–Xe^{++}, and elastic = Xe–Xe, Xe–Xe$^+$, and Xe–Xe^{++}. Elastic collisions between charged particles are not included in the model because collisions between charged particles are dominated by short-range coulomb interactions. To simulate short-range interactions, it is necessary to simulate many collisions that individually cause small angle deflections to occur but collectively cause large changes in particle trajectories. This requires simulating many collisions during each time step and is therefore computationally impractical. The mean cross section for momentum transfer caused by coulomb interactions is given in Mitchner and Kruger[13] and gives mean free paths greater than 20 m for both ion–ion and electron–electron collisions. The impact of this restriction is therefore negligible in this application.

To simulate a given collision process, it is necessary to know the velocity-dependent collision cross section. The Xe–Xe$^+$ CEX collision cross section is given by Rapp and Francis as[18]

$$\sigma_{\text{CEX}} = (k_1 \ell n\, c_r + k_2)^2 \times 10^{-20} \quad \text{m}^2$$

Where $k_1 = -0.8821$, $k_2 = 15.1262$, and c_r is in m/s. The Xe–Xe^{++} CEX cross section for the exchange of two electrons has been measured experimentally.[19] A logarithmic fit to the measured cross section gives

$$\sigma_{\text{CEX}} = (3.4069 \times 10^{-9} - 2.7038 \times 10^{-10} \ell n\, c_r) \quad \text{m}^2$$

The cross section for CEX between single and double ions has also been measured and is almost an order of magnitude smaller than the double ion–neutral CEX cross section; it is therefore neglected. When a simulated CEX collision occurs, the ion and neutral particle velocity vectors are exchanged to create a *slow* ion and a *fast* neutral. If the simulated collision partners have different macroparticle weights, an additional Monte Carlo selection is made to determine whether the velocity of the particle with the higher weight should be modified.[17] This ensures that the total energy and momentum are statistically conserved over many collisions.

Neutrals in the plume region undergo many types of elastic collisions. In general, the mean free path for these processes is large with respect to features of interest. Nevertheless, for completeness, some elastic collisions are included in the simulation. The variable soft sphere (VSS) model is used for Xe–Xe neutral collisions in the SPT plume[20]:

$$\sigma_E = (2.117 \times 10^{-18}\, c_r^{-0.24}) \quad \mathrm{m}^2$$

When a collision occurs, the scattering angle is also chosen using the VSS model:

$$\alpha = 1.107 c_r^{0.01944}, \qquad \chi = \cos^{-1}(2\beta^{1/\alpha} - 1)$$

New velocity vectors are determined using the equations for conservation of momentum and energy and Eq. (2).[15]

The collision cross section for $Xe–Xe^+$ elastic collisions can be derived analytically and is given by[21]

$$\sigma_E = (8.28072 \times 10^{-16}/c_r) \quad \mathrm{m}^2$$

According to theory, the ion mobility is independent of charge state, and so the $Xe–Xe^{++}$ elastic collision cross section is equal to twice the $Xe–Xe^+$ cross section.[22] When a neutral–ion collision occurs, the scattering angle is chosen randomly based on an isotropic scattering distribution. This is consistent with the dynamics of a hard sphere collision. As with CEX collisions, a Monte Carlo selection is made to determine whether the particle with the higher macroparticle weight is modified in a given collision. This ensures that the total energy and momentum are statistically conserved over many collisions.

Because the number of particles is limited by memory, as n_0/n_i approaches infinity, the ratio of the neutral particle weight to the ion particles weight also approaches infinity and total energy and momentum are no longer conserved. This has no impact on the validity of the simulation. When $n_i \ll n_0$, the momentum transferred from the ions to the neutrals has little effect on the neutral distribution function. In its extreme limit, the PIC–DSMC algorithm degenerates into a particle-in-cell–Monte Carlo collision (PIC–MCC) method. The PIC–MCC algorithm explicitly fails to conserve energy and momentum, even at a statistical level. However, the PIC–MCC method is a well-established method that has been shown to be valid in applications where $n_0 \gg n_i$

It is computationally impractical to simulate Xe–Xe elastic collisions when a neutral background is present in the simulation, and so these collisions were not included when simulating ground-based experiments. The difficulty comes from the need to mix particles with different macroparticle weights. When simulating a relatively dense neutral background, a larger macroparticle weight must be used for the neutrals than that used for ions, to keep the background particles from overwhelming the ions present in the simulation. However, when a simulated collision occurs, the size of the local collision time step is proportional to the macroparticle weight. Because the neutral macroparticle weight is much greater than the ion macroparticle weight, Xe–Xe collisions produce collision time steps much larger than those produced by Xe–ion collisions. Each neutral–neutral collision results in a collision time step equivalent to hundreds of simulation time steps. The resulting time-scale mismatch makes it impossible to efficiently simulate these collisions using a DSMC model. Xe–Xe collisions are therefore included only in simulations where the neutral background is not present, i.e., where the neutral macroparticle weight is approximately equal to the ion macroparticle weight. Because the neutral background is Maxwellian by assumption, this has little influence on results produced by the simulation.

Particles are loaded into the simulation at each time step to simulate the exit flow from a Hall thruster. The ion distribution is determined from an empirical model developed from experimental measurements of the ion current density 4 mm from the thruster exit.[5] These measurements give the magnitude and direction of the ion current as a function of radial position at an unspecified propellant flow rate. We found that the measured current density can be described by the following functions:

$$\alpha = 1730 - 2.30 \times 10^5 r + 1.06 \times 10^7 r^2 - 2.05 \times 10^8 r^3 + 1.45 \times 10^9 r^4 \tag{5}$$

$$j = -1210 + 8.40 \times 10^4 r - 1.78 \times 10^6 r^2 + 1.18 \times 10^7 r^3 \tag{6}$$

A model for the ion distribution is derived by assuming that ions leave the thruster with a drift velocity of 17,020 m/s in the r/z plane. This corresponds to the I_{sp} of an SPT-100 after excluding the flow to the cathode.[4] Variations in current density are assumed to correspond to variations in number density. Equation (6) is normalized by the integrated beam current to give

$$\beta = 2.55 - 1.67 \times 10^4 r^2 + 7.71 \times 10^5 r^3 - 1.23 \times 10^7 r^4 + 6.50 \times 10^7 r^5 \tag{7}$$

Equation (7) gives the probability that an ion crossing the exit plane has a radial position less than r. A random number β is chosen between 0 and 1. Equation (7) is then inverted computationally to give the particle's radial position. Once the position is determined, Eq. (5) determines the particle's divergence angle. The thermal velocity components are added in the axial and radial direction based on temperatures of 34 eV and 8000 K, respectively. The axial temperature is chosen to simulate the presence of a high-energy tail of ions that is seen in laboratory measurements of the ion distribution function. This point is discussed in detail in the section titled Retarding Potential Analyzer Measurements. The radial temperature is a reasonable estimate. The particle's tangential velocity is determined independently by assuming a drift velocity of 250 m/s and a temperature of 800 K. These values match measurements made by Manzella.[1]

Approximately 10% of the propellant entering an SPT-100 is diverted to the cathode. Because the cathode cannot be directly modeled in an axisymmetric geometry, the propellant that normally flows through the cathode is assumed to flow through the anode as unionized propellant. The neutral distribution in the plume has not been measured, and so the neutrals are assumed to have a temperature of 1000 K and are choked at the thruster exit.

Three-Dimensional Model

The axisymmetric model has been extended to simplified three-dimensional geometries and can be used to simulate relatively realistic spacecraft geometries. The model is based on an embedded Cartesian mesh, and so all surfaces must be flat and lie along Cartesian planes. The equations of motion are identical to Eq. (3c) in all three directions. A generic model of a communications satellite is used in this work. A simulated bus, yoke, and solar array are shown on a $3.2 \times 4.4 \times 3.2$ m computational domain. An embedded grid is used along the edge of the main bus. This grid is colocated with the thruster and is used to better resolve the core of the plume region. The

section of bus shown has dimensions of 1.1 × 1 × 2.6 m and represents a quarter of the spacecraft's main bus. A 1.9-m yoke connects the bus to the bottom of a solar array. The array is 1.0 m wide, and only the bottom 1.4 m of the array are included in the simulation. There are several limitations on the types of geometries that can be included in the three-dimensional plume model. First, all surfaces in the domain must be grid conforming. This precludes the use of curved surfaces to model antennae. Second, the weighting functions used along the boundaries between two solid objects that directly touch each other are calculated as though only one object is present. As a result, both charge and neutral densities are calculated incorrectly along the line that intersects both objects. The accuracy of the simulation away from the boundary is not affected. Third, the resolution of embedded grids is fundamentally limited by the underlying particle simulation. In computational fluid dynamics, embedded meshes are often used to resolve areas of interest. In particle simulations, adding an embedded mesh without increasing the number of particles results in fewer particles per cell and reduces the accuracy of the simulation. Particles must be added along with the mesh to obtain better resolution. In practice, the number of particles that can be added to a simulation is generally restricted by available memory. Embedded grids can be used in areas of high density, such as the core of the plume, but cannot be used to provide better resolution of objects in the far field.

One issue of particular interest to satellite designers is plume-induced deposition and/or erosion on sensitive parts of the spacecraft. Previous work has shown that eroded metal from the acceleration grids of ion thrusters can lead to deposition on solar cell cover glasses.[21] The anode of an SPT thruster undergoes substantial erosion, but the material released is a ceramic boron nitride compound and is unlikely to react with exposed surfaces. Because the propellant is a noble gas, we neglect plume-induced deposition in our surface model. This assumption is consistent with experimental results,[7] but may not be valid if metal surfaces are exposed to the plasma in the acceleration channel (as with TAL thrusters).

The ions in the plume are known to cause sputtering on exposed surfaces.[23] A surface-sputtering model has been developed and incorporated into the PIC–DSMC model. In the axisymmetric model, sputtering erosion rates are calculated by recording the flux and energy of macroparticles crossing an arc at a fixed distance from the anode exit. The surface is virtual, and so ions in the simulation continue on as though the surface were not present. This causes the simulation to slightly underestimate the acceleration of ions in the presheath, but has little impact on the final result.

In three-dimensional geometries, particles crossing an object boundary are removed or reflected at the boundary. Ions are neutralized and removed from the simulation while neutrals are reflected back into the domain in a manner consistent with an ideal specular surface. Objects like solar panels are represented as objects of fixed potential. Different points on the array can be assigned different potentials to mimic the distribution of cells across the array. In this work, the entire array is assumed to float at a uniform negative potential with respect to the plasma. Thermal blankets and other electrically isolated objects are represented as floating surfaces at the plasma's floating potentials. Their potential is determined by balancing the local flux of ions and electrons to the surface.

When a plasma interacts with an object, a sheath typically forms near exposed surfaces.[8] Figure 2 shows the structure of the sheath near a surface that is at the floating potential, which is negative with respect to the local plasma potential. This sheath is a non-quasi-neutral region with a width on the order of the Debye length. The present PIC–DSMC model is quasi-neutral by assumption, and cannot directly simulate this region. Fortunately, modeling the sheath itself is unnecessary. The Bohm sheath criterion requires that ions entering the sheath must be moving faster than the ion acoustic velocity. Once an

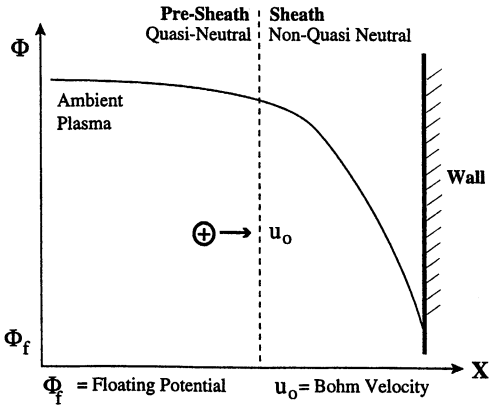

Fig. 2 Plasma potential profile near a solid surface at the floating potential.

ion enters the sheath, it is continuously accelerated until it strikes the wall. The sheath/presheath boundary serves as a sink into which ions disappear and never re-emerge. When a simulated particle leaves the presheath and enters the sheath, it is assumed never to re-emerge and the ion is removed from the simulation. The situation is analogous to a choked flow through a rocket nozzle. Because no information passes from the sheath back into the presheath region, it is possible to simulate flow up to the presheath boundary without simulating the detailed structure of the sheath itself. The detailed structure of the sheath and the wall potential have no effect on the overall structure of the plume.

For surfaces of fixed potential, the boundary conditions are more complex. When the surface potential is less than the local plasma potential, the situation is similar to that of a surface at the floating potential. Particles in the presheath do not interact with particles in the sheath and the magnitude of the potential drop is irrelevant. When the surface potential is greater than the local plasma potential, the electric field is reversed and the sheath attracts electrons. This creates substantial electron flow from the presheath into the sheath region. At high electron drift velocities, the Boltzmann relationship and the quasineutral PIC–DSMC formulation are no longer valid. We therefore require that surfaces of fixed potential sit at a negative potential with respect to the ambient plasma.

The analytic surface model is only valid when conventional one-dimensional sheath theory applies. This is the case when the Debye length is much less than the length scale of the surface (a restatement of the quasineutral assumption). The surface model is invalid in wakes and other regions of low charge density, and errors may be introduced along leading edges if the plasma flow is primarily parallel to the surface of interest.[24]

Sputtering rates are calculated by tabulating the material removed by each ion and neutral striking the surfaces of the spacecraft. The material loss is determined by multiplying an energy-dependent sputtering coefficient by the macroparticle weighting factor. Multiple materials are simulated by tracking separate sputtering coefficients. A particle's impact energy is given by the sum of its kinetic energy and the energy it gained or lost in the sheath. All particles are assumed to strike normal to the surface and neutrals undergo no acceleration in the sheath region. The sheath drop is calculated differently on fixed and floating surfaces. On fixed surfaces, the drop is determined by subtracting the surface potential from the local plasma potential. On floating surfaces, the drop is determined from one-dimensional sheath theory:

$$\phi = (kT_e/e)\ell n(4\Gamma_i/n_{\text{ref}}\bar{c}_e)$$

In the axisymmetric model, the collected flux and energy information are postprocessed to determine the magnitude of the

sheath drop that would be present on a surface sitting at the floating potential. In the three-dimensional model, the sheath drop is calculated as the simulation runs. The sheath drop is added to the recorded macroparticle energy to give the impact energy of ions on the surface. Once the impact energy is known, the amount of material removed is determined using an energy-dependent sputtering coefficient. This coefficient is material dependent and must be determined by experiment. Because Xe is the dominant species in the plume region, only Xe-induced sputtering is considered in this model. One material of interest to designers is silver, which is used to make solar-cell interconnects. Its sputtering coefficient is given by[25]

$$S = 7.334 \times 10^{-3}E - 0.29511$$

Another material of interest is the glass used to cover solar cells. Solar cell cover glasses are covered by a thin antireflective coating whose sputtering coefficient has not been reported in the general literature. The exact composition of the cover glass varies, but the sputtering coefficient for argon on quartz glass is used to represent a generic glass surface. It is given by[7]

$$S = 7.105 \times 10^{-4}E - 0.01815$$

Because quartz glass is harder than regular glass, this underestimates the actual erosion rate. The sputtering coefficient for the antireflective coating present on the cover glass is unknown. In all cases, the sputtering coefficient used is for xenon ions striking normal to the surface. It has been observed that the atoms striking at nonnormal angles may have higher sputtering coefficients than those striking normal to the surface.[26] At the present time, the angular dependence for xenon sputtering silver and quartz is unknown for low-energy ions. As a result, the surface model tends to underpredict the erosion rate. Better experimental measurements of the sputtering coefficient are needed to improve the surface model.

In summary, a PIC–DSMC simulation has been constructed, based on the observation that the plume is a quasineutral, unmagnetized plasma in which the electrons are effectively collisionless. The DSMC method is used to simulate collisional phenomena, and an empirical source model is used to simulate an SPT-100 thruster. The plume simulation was written in ANSI C, and runs were carried out on UNIX workstations with 96-256 Mbytes of RAM. Run times were typically 2–4 h for axisymmetric geometries and 12–20 h for the three-dimensional geometries.

Axisymmetric Results

The results of the axisymmetric plume simulation were tested for numerical consistency and compared with several types of experimental data. A common test for numerical accuracy in PIC simulations is to verify that the total energy in the simulation is conserved over time. This was confirmed numerically in our PIC–DSMC model over thousands of iterations. Because CEX collision dynamics are relatively simple, the primary issue with the DSMC model is to properly simulate collision frequencies within a mixed gas. This was tested by simulating a collimated beam of neutrals entering a background neutral gas. The simulated collision frequencies were compared to theory and shown to be accurate. Further numerical tests confirmed that the results were insensitive to the number of particles in the simulation and to the number of the iterations once the plume had reached a steady state.

Ion Current Density

The PIC–DSMC plume model can be used to model SPT thrusters operating in a neutral background gas. It is therefore possible to directly simulate the condition present in ground-based plume experiments. Direct comparisons have been made to measurements taken specifically for this work at the University of Michigan and to previously reported measurements taken at NASA Lewis in 1994. The University of Michigan vacuum facility consists of a 6-m by 9-m chamber and can pump approximately 30 kl of xenon per second.[27] A Faraday probe was used to measure the ion current density in the plume along an arc 50 cm from the exit of an SPT-100 thruster. The measured background pressure in the University of Michigan facility was 5.2×10^{-5} torr. An axisymmetric simulation has been carried out to duplicate this experiment on the computational domain shown in Fig. 3. The grid cells are 10 cm on a side (5 cm near the core of the plume), and a total of 100,000–200,000 particles were used in each simulation. The presence of background gas is simulated by adding neutral xenon particles in a Maxwellian distribution and by including thermal xenon fluxes along boundaries with the ambient plasma. The background neutral temperature is assumed to be 300 K, and the number density is determined using the ideal gas law. Simulations were also carried out on higher-resolution grids and on grids with different levels of embedded meshes to confirm that the results were grid independent. Figure 4 compares the simulated and experimental ion current density as a function of angle from the plume centerline. The error bars on the data are estimated to be approximately 35%. Most of this error (25%) is a result of uncertainty in the measurement of the background pressure in the test chamber. The rest is a result of uncertain knowledge of the effective collection area of the Faraday probe, secondary electron emission from the probe, and ambient stray currents in the facility. These errors scale directly with ion current density, and so the error bars are constant throughout the range of measurement. The results agree qualitatively with experimental results, but show only fair agreement in terms of magnitude. The simulated ion current density is consistently within 50% of the experimental results across the domain, except for a small region near the centerline. The disagreement between the model and experiment is a result of experimental error, a 20% uncertainty in the CEX ion cross section, and uncertainty in the SPT source

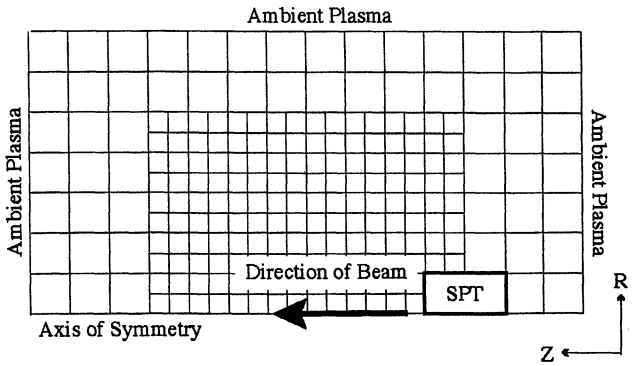

Fig. 3 Grid and domain.

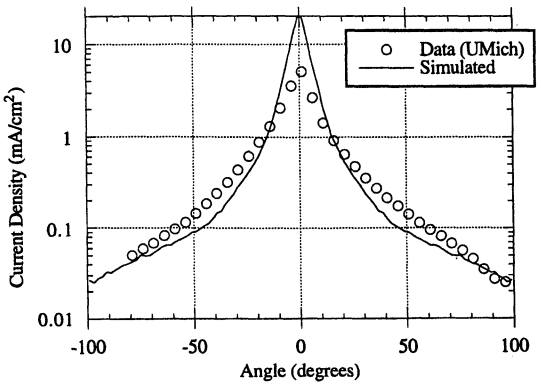

Fig. 4 Simulated and measured ion current density ($P = 5.2 \times 10^{-5}$ torr).

model. The disagreement at the centerline is larger, approximately by a factor of 3, and is probably a result of approximations made in the source model. Overall, the simulation shows fair agreement with the measured data.

Measurements of ion current density taken by Manzella[4] at NASA Lewis were made using a 5 by 19 m chamber with a xenon pumping rate of 500 kl/s. The current was measured 60 cm from the exit of an SPT-100 thruster at four different background pressures. These measurements are shown in Fig. 5. As one would expect, higher ambient pressures result in higher backflow currents because of a higher CEX collision rate. Even at the lowest achievable pressures, backflow still occurs because of CEX collisions with the background gas and with unionized propellant. The PIC–DSMC model allows one to estimate the actual backflow under orbital conditions. A comparison of the simulated and measured ion current densities at a pressure of 2.2×10^{-6} torr shows only qualitative agreement. The simulation consistently underpredicts the ion current, except very close to the centerline. As a result, the integrated beam current is much larger in the experimental case than it is in the simulation. Interestingly enough, the experimentally measured current is also larger than the actual current being emitted by the thruster. The following paragraph compares the experimentally measured thruster discharge current with beam currents derived by integrating the Lewis data.

Because the discharge current provides the electrons necessary to neutralize the beam, it is not possible for the beam current to exceed the actual discharge current. Because the measured beam currents exceeds the discharge current by between 4 and 33%, an external current source must be affecting current density measurements. By contrast, when the integrated beam current is calculated from the Michigan data shown in Fig. 4, the result is 3.55 A. This value is less than the discharge current and is therefore physically consistent.

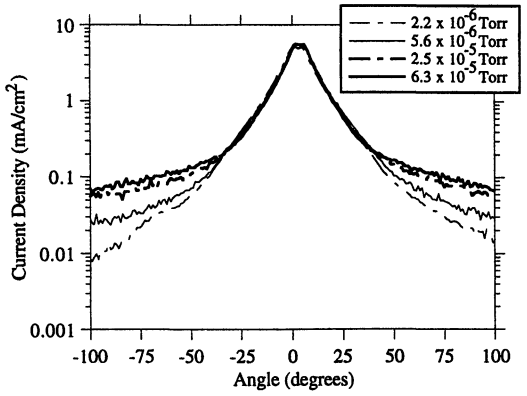

Fig. 5 Measurements of ion current density as a function of facility pressure (z = 60 cm).[8]

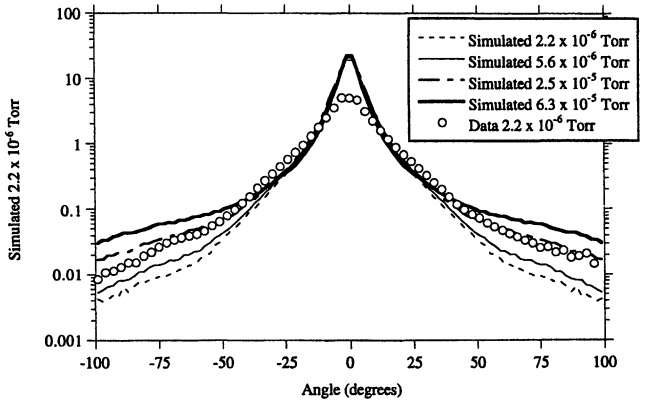

Fig. 6 Simulated and measured ion current density with external current included in model.

The amount by which the beam current exceeds the expected value in the following text varies with pressure, suggesting that an interaction is occurring with the ambient background. Pressure = 2.2×10^{-6}, 5.6×10^{-6}, 2.5×10^{-5}, and 6.3×10^{-5} torr. Current = 4.69, 5.26, 5.97, and 6.15 A. Discharge current = ~4.5 A. It is likely that the background plasma in the chamber is undergoing recirculation and creating an artificial ion current. To examine the impact of the external current source on our results, simulations were conducted in which the anode ion flow was increased by the difference between the thruster's nominal current and the beam currents given earlier. The simulated results at a pressure of 2.2×10^{-6} torr are shown in Fig. 6. Also shown are measurements taken at NASA Lewis Research Center at four different tank pressures.

Figure 6 shows better agreement with data. Overall, the same shapes and trends are present in Figs. 5 and 6, and the results have fair numerical agreement, within a factor of 2–3 across the domain with larger disagreement at very high and low angles. The simulated results consistently overpredict the current along the centerline and underpredict it at high angles. The underprediction at high angles may be caused by the ambient plasma in the test chamber. Because the current measured at high angles is relatively small, these measurements may be disproportionately affected by the recirculating plasma. This effect is not accounted for in the corrected simulation. The underprediction could also be caused by errors in the measured CEX cross sections, which is estimated at 20%,[18] or may result from assumptions in the source model.

In summary, the results of the axisymmetric PIC–DSMC plume simulation have been compared with two separate measurements of the ion current density. The results agree qualitatively with data taken at the University of Michigan and are within the experimental and modeling uncertainty, except near the centerline. The results also agree qualitatively with data taken at NASA Lewis Research Center at background pressures that vary by an order of magnitude.

Erosion Rates

To verify the surface interaction model, the results from the PIC–DSMC model were compared with experimentally measured erosion rates from Randolph et al.[7] Randolph placed samples of silver foil, solar cell interconnects, and solar cell cover glasses in a vacuum tank and exposed them to the SPT-100 plume for a period of 200 h. The experiments were conducted at a pressure of 3×10^{-5} torr, and collimators were used to protect the samples from contamination. Figure 7 shows experimental and simulated results for the erosion of silver after 200 h of exposure at a pressure of 2.5×10^{-5} torr as measured 1 m from the thruster exit. Although the simulated results are noisy, they agree fairly well with the experimental data. The shapes and trends show good qualitative agreement. However, the simulation consistently underpredicts the measured erosion rate, sometimes by more than a factor of 2. Fig-

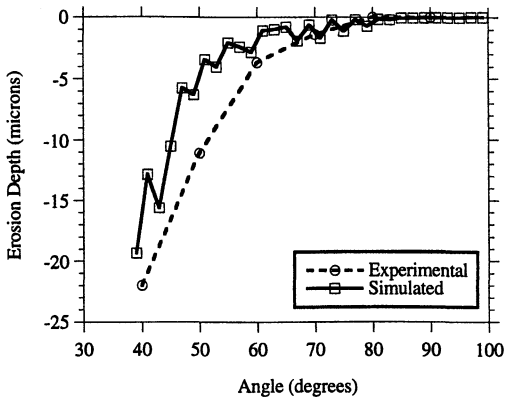

Fig. 7 Comparison of calculated silver erosion rates and experimental measurements.

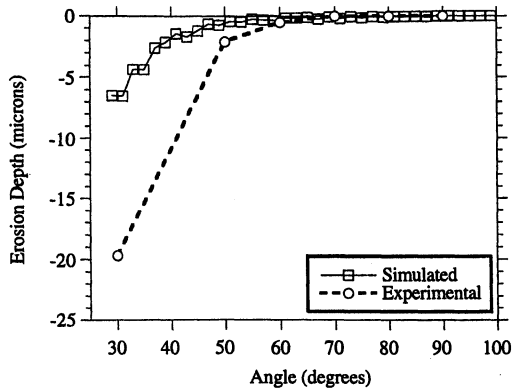

Fig. 8 Comparison of calculated coverglass erosion rates and experimental measurements.

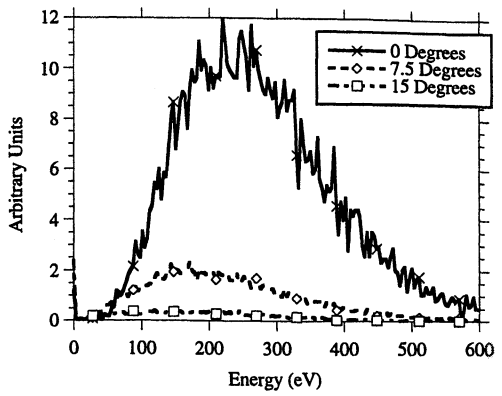

Fig. 9 Simulated ion energy distribution.

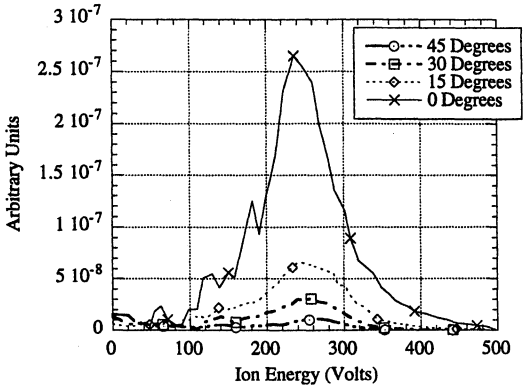

Fig. 10 Measured ion energy distribution.

ure 8 shows similar results for the erosion of Quartz after 200 h of exposure. Also shown is the experimentally measured erosion of solar cell cover glasses after 200 h of exposure. Although the same trends are apparent, the agreement is not very good and the simulation consistently underpredicts the data by a factor of 3 or more. The relatively high quality of the results shown in Fig. 7 and the low quality of the results in Fig. 8 suggests that the erosion model is sensitive to the relationship used to represent the sputtering coefficient. The material used in the solar-cell cover glasses most likely has a higher sputtering coefficient than the quartz glass simulated in the surface model. This causes the simulation to significantly underpredict the erosion rate of solar-cell cover glasses. An additional source of error is that the sputtering coefficients used in the simulation are for ions striking normal to the surface. Ions that approach at high angles can have sputtering coefficients several times higher than those striking normal to the surface, leading to higher erosion rates than predicted by the PIC–DSMC model.[11] Unfortunately, no data are available on the angular dependence of the sputtering coefficient of xenon atoms on silver or solar-cell cover glasses. Such data are necessary to further refine the sputtering model.

Questions of interest to designers are how much damage the plume will cause to satellite surfaces and how the erosion rate scales with distance from the anode exit. Analysis of the simulation results for silver and quartz glass surfaces placed at varying distances from the exit of an SPT-100 operating in vacuum, shows that they scale as a $1/z^2$ scaling law. The estimated erosion rate varies very strongly with angle from the centerline and varies by roughly an order of magnitude for each 20-deg change in angle. This indicates that a thruster's angle with respect to a surface will have a great impact on the erosion rate and that spacecraft designers will have to cant the thruster away from sensitive surfaces to prevent plume-induced erosion. The results also suggest that observed erosion rates can be scaled using a $1/z^2$ law, and these results combined with this scaling law to produce quick estimates of the erosion rate at a given position in the plume. Designers can also use the relationship to scale experimentally measured erosion rates to areas far from the thruster exit.

Retarding Potential Analyzer Measurements

A retarding potential analyzer (RPA) has been used to measure the ion energy distribution in the plume.[28] The simulated ion distribution is measured by recording the energy of macroparticles crossing a fixed imaginary surface. The results are shown in Fig. 9. It is constructed by recording the energy of particles crossing an arc 60 cm from the anode exit in increments of 0.5 deg. Figure 10 shows experimental RPA measurements taken at the University of Michigan at a pressure of 5.2×10^{-5} torr. The overall level of agreement between simulation and experiment is not very good. The peak in the simulated data is broader than in the experiment. This is a result of the 34-eV axial ion temperature used in the simulation. The actual ion temperature can be estimated by measuring the width of the peak in the RPA data and assuming a Maxwellian distribution. When the Maxwellian distribution is written in terms of energy, it takes the form

$$f(\varepsilon) = \left(\frac{m_i}{2\pi k T_i}\right) \exp\left[-\left(\frac{\sqrt{\varepsilon} - \sqrt{E_b}}{\sqrt{T_i}}\right)^2\right]$$

$$\varepsilon \equiv \frac{\frac{1}{2} m_i v^2}{e}, \qquad E_d \equiv \frac{\frac{1}{2} m_i v_b^2}{e} \tag{8}$$

Equation (8) describes a nonsymmetric peak whose width depends on the ion temperature and drift velocity. In Fig. 10, the peak of the distribution function is at an energy of 236 V. This is designated as the drift energy (E_d = 236 eV). From Eq. (8), when

$$(\sqrt{\varepsilon} - \sqrt{E_d})/\sqrt{T_{ev}} = 1$$

the height of the distribution function is 0.37 times its peak value. In Fig. 10, the distribution is 0.37 times its peak value when the collector potential is 305 and 181 V, resulting in ion temperatures of 4.42 and 3.64 eV, respectively. These values are consistent with previous measurements[1] and differ from each other because the ion distribution is not a true Maxwellian. The ion temperature used in the simulation is an order of magnitude higher than these estimates, and so it is no surprise that the simulated peak is wider than the experimentally measured distribution function.

The problem with this method of calculating the ion temperature is that it fails to account for the high-energy *tail* present in Fig. 10. This tail contains ions with energies hundreds of volts above the 300-V cathode–anode drop. The reason that this tail occurs is unknown, but it may indicate that plasma instabilities play a role in the creation of high-energy ions. This

population of ions is important to the overall plume structure. A axial ion temperature of 34 eV is used in the simulation to provide a population of high-energy ions. The result gives better agreement to the observed structure of the ion current density than simulated temperatures less than 10 eV. When the ion temperature is less than 10 eV, the ion current density takes on a wing structure that is not seen in SPT-100 laboratory data, but is characteristic of the plumes from gridded ion thrusters.[29]

In summary, the high-energy ion tail seen in Fig. 9 is a consequence of the assumed axial ion temperature. The simulation offers no direct insight into the mechanism by which the SPT-100 creates these high-energy ions, and work is needed to understand the physical mechanism by which these ions are created and the role instabilities play in the SPT-100 thruster.

The location of the peak in the simulated data varies with the RPA's angle from the centerline. This effect is not seen in the laboratory data. The shift is caused by the plume expansion and is related to the turning radius of ions leaving the thruster. The density gradient at the edge of the plume creates an electric field that turns ions away from the centerline at a rate related to their initial velocity. Ions with higher velocities have larger turning radii and tend to follow straighter trajectories. As the plume expands, high-energy ions tend to cluster along the centerline, whereas low-energy ions are turned toward the edges of the plume. This causes the location of the peak to shift downward with increasing divergence angle, an effect that is visible in the simulated data. However, the experimental measurements show no shift in the energy of the peak. In fact, although the magnitude of the peak drops rapidly, the location of the peak is virtually identical at all divergence angles. Experimental evidence for the existence of these high-energy ions at large divergence angles has been recently reported.[30] These ions appear because at large distances the thruster acts as a spherical cold source of ions and the potential drop through the plume is not sufficiently large to cause a significant shift in the energy of the ions.

In summary, the PIC–DSMC model presented in this paper has been compared with several sets of experimental data. The model shows reasonable qualitative agreement with ion current density data, but compares less well to RPA data. A sputter erosion model has also been described and compared with experimental data. This model shows good agreement with measured erosion rates for silver interconnects, but is less accurate when predicting the erosion of solar-cell cover glasses. More accurate measurements of cover glass sputtering coefficients are needed to improve these results.

Simulation of Thruster in Vacuum

Ground-based tests are carried out in vacuum chambers where the quality of the vacuum is limited by the facility's pumping speed. Tests on the SPT-100 thruster are typically carried out at pressures around 3×10^{-5} torr, though pressures as low as 2×10^{-6} torr can be achieved in some facilities. Figure 11 shows several plots of the ion current density 60 cm from the exit of an SPT-100 thruster. The top two lines show the experimental and simulated ion current density at a pressure of 5.2×10^{-5} torr. The next line shows simulated results for a thruster operating at 2.2×10^{-6} torr (the lowest pressure presently achievable in ground facilities). The bottom line shows simulated results for a thruster operating in vacuum. This case cannot be duplicated in ground tests and represents a thruster operating in geostationary orbit where actual pressures are on the order of 10^{-10} torr. At high angles, the ion current density in vacuum is an order of magnitude lower than the simulated or measured current at 5.2×10^{-5} torr. This result demonstrates the effect that the neutrals present in ground-based tests can have on experimental measurements. The ambient background increases the CEX collision rate and significantly increases the backflow current. However, the simulated current of 2.2×10^{-6} torr is virtually identical to the simulated results in vacuum. At very low pressures, the neutrals from the thruster dominate the background gas and effectively control the CEX collision rate. We conclude that plume tests conducted at these pressures do give a relatively accurate picture of the plume's structure in vacuum. This conclusion should give designers confidence that ground-based tests in state-of-the-art facilities can accurately replicate the plume's structure under orbital conditions.

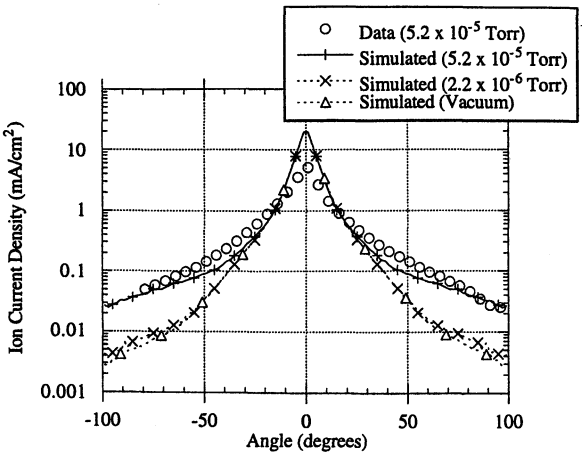

Fig. 11 Current density in ground test and in vacuum (pressure = 5.2×10^{-5} torr).

Three-Dimensional Results and Discussion

A three-dimensional PIC–DSMC plume model has also been developed and validated numerically and against experimental measurements. In all test cases, the three-dimensional simulation was confirmed to produce results virtually identical to the axisymmetric simulation and to compare equally well with experimental data. Numerical tests were applied to the three-dimensional model and it was shown to conserve total energy, and the results were shown to be insensitive to the number of iterations and the number of particles in the simulation. Comparisons were also made with results generated on higher-resolution grids to confirm that the solution is grid independent. One interesting aspect of the three-dimensional results is that the number of particles per cell varies drastically from 1600 per cell in the core of the plume to less than 5 per cell at the edges of the domain. Traditionally, both PIC and DSMC schemes require 10 particles per cell to retain statistical accuracy. However, when the three-dimensional results created with 3–1600 particles per cell are compared with axisymmetric results produced with 20–2000 particles per cell, the results are virtually identical. Having fewer than 10 particles per cell at the edges of the plume does not hurt the accuracy of the simulation. This is the case because the important physics occurs in the center of the plume, where the majority of the CEX collisions actually occur. Particles at the edges of the plume undergo relatively few collisions and follow almost ballistic trajectories. Numerical confirmation of this conclusion was reached by increasing the number of the particles in the simulation and observing that the results were still virtually identical to the axisymmetric case. Therefore, while it is important to maintain the number of particles per cell in the core of the plume, some latitude can be exercised in the outer parts of the three-dimensional simulation. Typically, about 1,000,000 particles were used in each of the three-dimensional plume simulations. The cells of the mesh are 12 cm long on each side, 6 cm near the core of the plume.

Once the code was validated, an effort was made to study the effect the plume would have on a realistic satellite configuration. Runs were conducted to simulate an SPT thruster used for N–S stationkeeping on the simple GEO communications satellite model discussed previously. The spacecraft is oriented

with the arrays on the N–S sides of the spacecraft, so thrusters operating for N–S stationkeeping fire in a vertical direction. This placement of the array relative to the thruster is typical for geostationary satellites. The SPT-100 thruster is mounted at the edge of the bus under the array as shown in Fig. 12. The array angle (α) is related to the rotation of the array about the N–S axis. Because of geometric limitations, the array cannot be directly rotated in the computational simulations. Instead, the thruster's location and orientation are used to simulate a given array and cant angle. The cant angle is the angle between the thrust vector and the vertical axis, and higher cant angles cause an effective loss of I_{sp} for stationkeeping. The array angle is defined as the solar panel's angle relative to an imaginary line connecting the yoke to the thruster and varies as the spacecraft orbits the Earth. All simulations were run for 15,000 time steps, with a time step of 0.1 normalized units. Because modern spacecraft use electrical systems based on approximately a 92-V bus voltage, the potential of simulated array was fixed at −92 V relative to the center of the plume. A real array would be covered by cells with varying potentials, but setting the entire surface to −92 V is a conservative assumption because it results in the highest impact energy for incoming plume ions.

A cant angle of 45 deg and an array angle of 45 deg were chosen as the spacecraft's baseline configuration. Figure 13 shows a planar cut through the baseline configuration showing contours of constant potential. The plume is clearly visible as a region of high potential located at the top of the bus. The plume emerges from the thruster, directly impacting the array and forming a wake region behind it. The quasineutrality breaks down in this wake region and the simulation is not valid in this area. Figure 14 shows a contour plot of ion current density on the face of the array nearest to the plume. Although the plot is noisy, a small but noticeable flux of ions is reaching

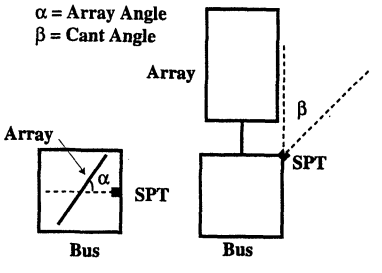

Fig. 12 Definition of cant angle and array angle.

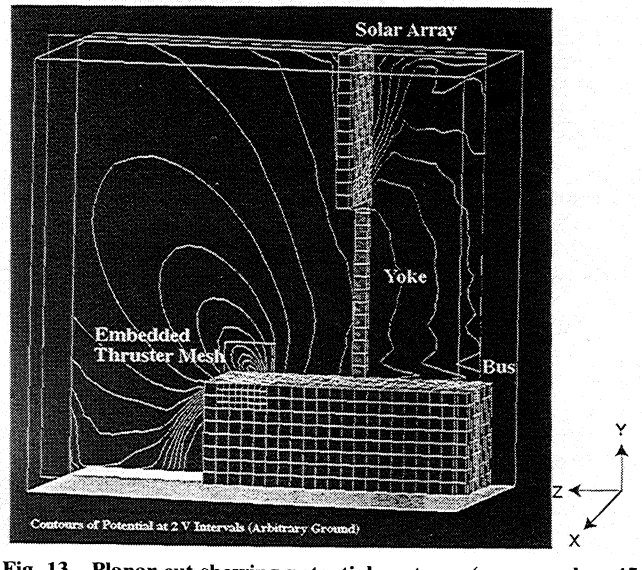

Fig. 13 Planar cut showing potential contours (array angle = 45 deg, cant angle = 45 deg).

the surface, even though the thruster is oriented away from the array. As one would expect, the area of highest flux is in the corner of the array that sits closest to the anode exit. Very little current reaches the lower or upper left corners of the array. Figure 15 shows the energy of ions striking the surface of the array. The ions with relatively high energies are actually striking the upper right corner of the array, whereas ions with relatively low energy strike the corner nearest the thruster. This occurs because ions emerging from the thruster at different energies have different turning radii. High-energy ions follow relatively straight trajectories and do not turn far enough to strike the lower part of the array. CEX ions, on the other hand, have a small turning radius and are easily influenced by electric fields at the edge of the plume. These ions turn quite sharply and end up striking the bottom of the array.

Figure 16 shows calculated erosion rates for silver surfaces on the array. All materials are assumed to sit at −92 V with respect to the center of the plume. This figure suggests that noticeable and potentially significant erosion will occur to interconnects on the solar array. As one would expect, the highest erosion rates occur on surfaces closest to the thruster. Silver, in particular, has an erosion rate greater than 1 μm per month in some parts of the array. The actual area over which these high rates occur is relatively small, an area of about 0.25 m^2. In addition, these surfaces are being held at a negative potential with respect to the plume. One way to lower the peak erosion rate is to bias cells at the corners of the array positive

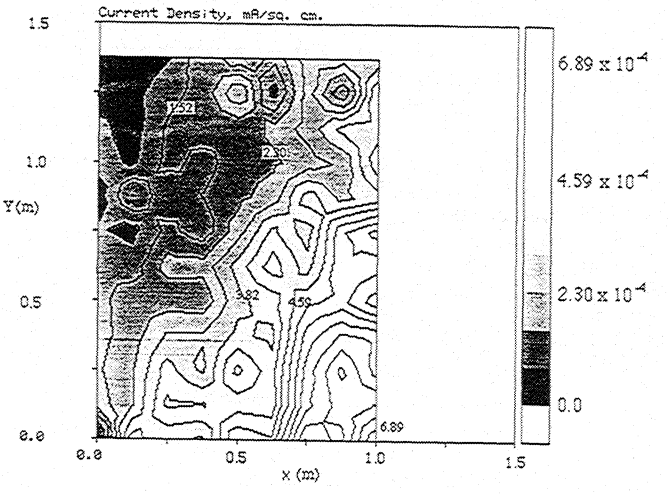

Fig. 14 Ion current density on surface of solar array (array angle = 45 deg, cant angle = 45 deg).

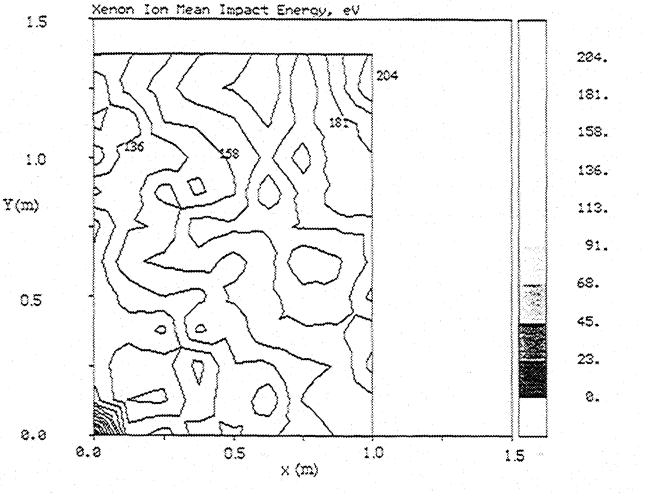

Fig. 15 Mean energy of ions striking solar array (array angle = 45 deg, cant angle = 45 deg).

with respect to the spacecraft. This lowers the energy of ions striking the surface of the array and mitigates sputtering losses. Another way to prevent damage is to incorporate a plume shield into the satellite design to deflect part or all of the plume away from the array.

The relationship of most interest to spacecraft designers is the relationship between the cant angle, array angle, and the erosion rates experienced on the array. Canting the thruster away from the satellite's N–S axis lowers the thruster's effective I_{sp}, and so it is desirable to use as small a cant angle as practical. A series of simulations were conducted at different cant and array angles used to produce a map of the relationship between these parameters. Results from 21 runs were extrapolated to other cant and array angles using weighted averages based on one-over-distance-squared weighting factors. The results are summarized in Figs. 17 and 18. Figure 17 shows the erosion rate experienced at the corner of the array that is closest to the thruster when the array angle is 90 deg. Figure 18 shows the erosion rate experienced at a point 20 cm from the bottom of the array and 20 cm from the side of the array, or about 30 cm away from the lower right corner. The upper left corners of these figures are significantly undersampled, but the cant and array angles in this quadrant are not generally of interest to spacecraft designers. As one would expect, lower cant and array angles result in higher erosion rates. The erosion rate varies by more than 2 orders of magnitude over the parameter space. From the plot, it is clear that silver interconnects will undergo some erosion over the lifetime of the satellite. The allowable cant and array angles for this configuration depend on the acceptable erosion rate and the amount of time the array will be exposed to the plume from the SPT thrusters. Determining these rates requires knowledge of the thruster configuration and duty cycle. As a baseline case, it is assumed that the thruster is used for N–S stationkeeping with a 2000-kg satellite in geosynchronous orbit over a lifetime of 12 years. The total Δv required is about 617 m/s.[31] It is also assumed that four thrusters are mounted on the satellite, two on the north and south faces, respectively. Each SPT-100 thruster produces 85 mN of thrust, but because the four thrusters are canted with respect to the array, the effective thrust is less than this value. An effective thrust of 60 mN was assumed for this analysis. The total thruster operation time is given by

$$t = m\Delta v/F$$

The resulting operation time is 2852 h (4.0 months) over a 12-year satellite lifetime. The solar array orientation changes continuously as the satellite travels around the Earth. Only one side of the array produces power, and because erosion rates are very small at array angles greater than 90 deg, each half of the array is exposed to the plume from an SPT thruster only half of the time. This gives an effective exposure time of 1426 h (2 months). The actual erosion that occurs over the spacecraft's lifetime will depend on the exact operational time and duty cycle of the SPT thrusters. To draw general conclusions, a simple parametric study has been conducted.

A typical solar cell interconnect is made of silver and is about 25 μm thick. When the interconnect erodes, the resistance in the connection increases and causes a power loss. Assuming that losses become significant when 10% of the interconnect's thickness has eroded, the allowable erosion depth is 2.5 μm (which translates to an average rate of 1.2 μm/month over the lifetime of the satellite). Figures 17 and 18 show the cant and array angles at which such rates can be achieved on the simulated spacecraft configuration. In Fig. 17, these regions are relatively small. Even at a cant angle of 45 deg, array angles greater than about 60 deg are required to avoid unacceptable erosion rates for the interconnects. This can be achieved by modifying the thruster duty cycle so that the thrusters only operate at these array angles. In fact, it may be possible to push the cant angle down to 40 deg and still achieve a mean erosion rate of 1.2 μm/month by operating the thrusters for only a short period of time during each orbit.

At high cant angles, only a small portion of the array is affected by the plume. Figure 18 shows the erosion rate at a point 30 cm away from the point shown in Fig. 17. The simulated erosion rates are lower because this point is located

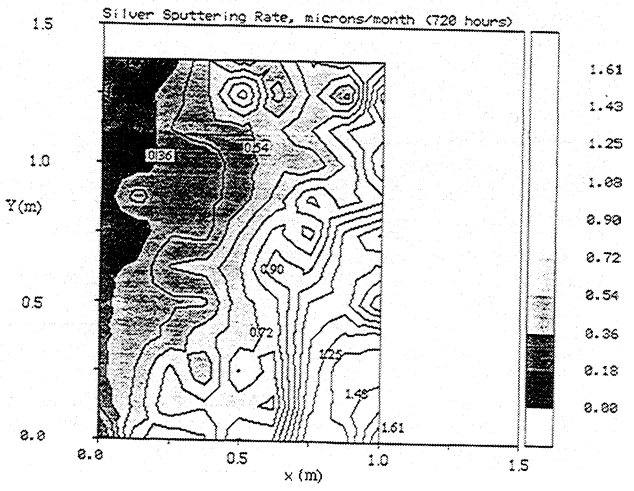

Fig. 16 Simulated erosion rate for silver (array angle = 45 deg, cant angle = 45 deg).

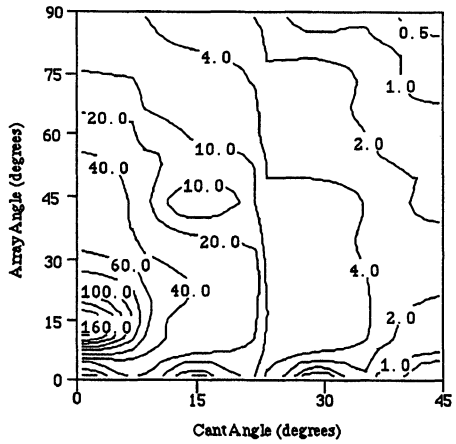

Fig. 17 Erosion rate for silver at corner of array. SPT-100 thruster, mass flow = 5.37 mg/s, I_{sp} = 1610 s, yoke length = 1.9 m, array width = 1.14 m.

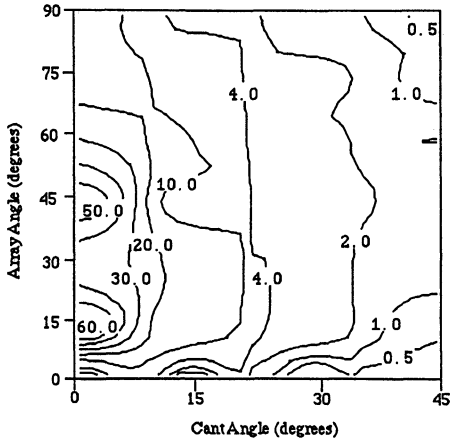

Fig. 18 Erosion rate for silver 0.3 m from corner of array. SPT-100 thruster, mass flow = 5.37 mg/s, I_{sp} = 1610 s, yoke length = 1.9 m, array width = 1.14 m.

farther away from the thruster. A mean rate of 1.2 μm/month can be achieved on this part of the array at cant angles of 35 deg or less with the proper duty cycle. Installation of a plume shield could allow the even lower cant angles.

Based on Figs. 17 and 18, we conclude that cant angles greater than 40 deg and array angles greater than 50 deg are acceptable for the satellite considered in this study. These results only consider the effects of the plume on array interconnects and depend on several assumptions. First, the simulated array is biased at -96 V with respect to the thruster. Portions of the array biased at positive voltages will experience lower erosion rates. In addition, the interconnects themselves sit between cells and may be partially shielded from the plume. On the other hand, the relatively small amounts of erosion that occur at array angles greater than 90 deg have been neglected, and nonnormal ion impact angles are not included in the present model. These factors must all be considered when applying the simulation to real configurations. Overall, interconnect erosion does not seem to be a fundamental barrier to the use of Hall thrusters on satellites. However, SPT thrusters will have to be canted with respect to the array, resulting in a lower effective specific impulse than the nominal value.

Conclusions

A computational model of an SPT plasma plume has been constructed using a quasineutral PIC–DSMC model. This model is based on theoretical work showing that the plume consists of a quasineutral plasma with collisionless electrons in which the magnetic field can be neglected. The resulting simulation models an SPT-100 plume on meter-length scales. Comparisons between the model and experimental data indicate that the PIC–DSMC simulation produces reasonable qualitative models of large-scale features in the plume. These features include the ion current density and the erosion rate for some materials exposed to the plume. However, comparison with RPA data show the limitations of the present model and highlights several questions about the SPT-100 thruster. The RPA data indicate that high-energy ions are present throughout the plume region, even in regions far from the centerline. The data also indicate that a tail of high-energy ions is present in the plume, which may imply that plasma instabilities play an important role in the creation of high-energy ions. Further work is needed to clarify the role instabilities play in the plume region. At the present time, the plume model is unable to replicate the ion distribution function in the plume.

Predictions have been made of the erosion rates that would be experienced by materials exposed to the plume, and a $1/z^2$ scaling law is suggested as a means of extending near-field sputtering measurements to far-field areas. Three-dimensional results are presented to demonstrate the model's ability to evaluate realistic spacecraft configurations. The results show the impact that the thruster's cant angle and the solar array position have on plume induced erosion. Both the erosion rate and the area of the array affected by the plume are shown to change dramatically with thruster and array orientation. The results also demonstrate that the three-dimensional model can be adapted and used by spacecraft designers to evaluate relatively realistic spacecraft configurations.

Overall, the PIC–DSMC algorithm presented in this paper has been shown to produce results that are qualitatively similar to measured experimental data. Future work is planned to improve the simulation and develop a tool for designers seeking to investigate the impact of SPT thrusters on spacecraft. New sputtering data will be incorporated into the surface interaction model as they become available, and efforts will be made to improve the source model to give better agreement with experimental data.

Acknowledgments

This paper was funded by the U.S. Air Force Office of Scientific Research under Grant F49620-95-1-0319. The authors thank David Manzella at NYMS Inc. for providing data used in this paper, Tom Randolph at Space Systems Loral for data and help with the satellite geometry, and Manuel Martinez-Sanchez at MIT for his insight and help.

References

[1]Manzella, D., "Stationary Plasma Thruster Ion Velocity Distribution," AIAA Paper 94-3141, June 1994.

[2]Absalamov, S. K., et al. "Measurement of Plasma Parameters in the Stationary Plasma Thruster (SPT-100) Plume and its Effect on Spacecraft Components," AIAA Paper 92-3156, July 1992.

[3]Myers, R. M., and Manzella, D. H., "Stationary Plasma Thruster Plume Characteristics," International Electric Propulsion Conf., Paper 93-096, Sept. 1993.

[4]Manzella, D. H., and Sankovic, J. M., "Hall Thruster Ion Beam Characterization," AIAA Paper 95-2927, July 1995.

[5]Gavryushin, V. M., and Kim, V., "Effect of the Characteristics of a Magnetic Field on the Parameters of an Ion Current at the Output of an Accelerator with Closed Electron Drift," *Soviet Physics—Technical Physics*, Vol. 26, No. 4, 1981, pp. 505–507.

[6]Dickens, J., Kirstiansen, M., and O'Hair, E., "Plume Model of Hall Effect Plasma Thrusters with Temporal Consideration," International Electric Propulsion Conf., Paper 95-171, Sept. 1995.

[7]Randolph, T., Pencil, E., and Manzella, D., "Far-Field Plume Contamination and Sputtering of the Stationary Plasma Thruster," AIAA Paper 94-2855, July 1994.

[8]Bishaev, A. M., Kalashnikov, V. K., and Kim V., "Numerical Modeling of Rarefied Plasma Plume Entering Neutral Environment Gas," International Electric Propulsion Conf., Paper 93-197, Sept. 1993.

[9]Arkhipov, B. A., and Kozubsky, K. N., "The Development of the Cathodes-Compensators for Stationary Plasma Thrusters in USSR," International Electric Propulsion Conf., Paper 91-023, Oct. 1991.

[10]Chen, F. F., *Introduction to Plasma Physics and Controlled Fusion, Volume 1: Plasma Physics*, Plenum, New York, 1984.

[11]Chapman, B., *Glow Discharge Processes*, Wiley, New York, 1980.

[12]Banks, P., "Collision Frequencies and Energy Transfer, Electrons," *Planetary and Space Science*, Vol. 14, 1966, pp. 1085–1101.

[13]Mitchner, M., and Kruger, C., *Partially Ionized Gases*, Wiley, New York, 1973.

[14]Birdsall, C. K., and Langdon, A. B., *Plasma Physics Via Computer Simulation*, Adam Hilger, Bristol, England, UK, 1991.

[15]Bird, G. A., *Molecular Gas Dynamics*, 1st ed., Clarendon, Oxford, England, UK, 1976.

[16]Ruyten, W. M., "Density-Conserving Shape Factors for Particle Simulations in Cylindrical and Spherical Coordinates," *Journal of Computational Physics*, Vol. 105, 1993, pp. 224–232.

[17]Elgin, J. B., "Getting the Good Bounce: Techniques for Efficient Monte Carlo Analysis of Complex Reacting Flows," Spectral Sciences, Inc., TR SSI-TR-28, Burlington, MA, 1985.

[18]Rapp, D., and Francis, W. E., "Charge Exchange Between Gaseous Ions and Atoms," *Journal of Chemical Physics*, Vol. 37, No. 11, 1962, pp. 2631–2645.

[19]Hasted, J. B., and Hussain, M., "Electron Capture by Multiply Charged Ions," *Proceedings of the Physical Society, London*, Vol. 83, 1964, pp. 911–924.

[20]Koura, K., and Matsumoto, H., "Variable Soft Sphere Molecular Model for Air Species," *Physics of Fluids A*, Vol. 4, No. 5, 1992, pp. 1083–1085.

[21]Samanta Roy, R. I., "Numerical Simulation of Ion Thruster Plume Backflow for Spacecraft Contamination Assessment," Ph.D. Dissertation, Dept. of Aeronautics and Astronautics, Cambridge, MA, June 1995.

[22]Dalgarno, A., McDowell, M. R. C., and Williams, A., "The Mobilities of Ions in Unlike Gases," *Philosophical Transactions of the Royal Society of London*, Vol. 250A, No. 982, 1958, pp. 51–425.

[23]Peng, X., Ruyten, W., and Keefer, D., "Comparison of 2D and 3D Models of Grid Erosion in an Ion Thruster," AIAA Paper 91–2120, July 1991.

[24]Wang, J., "Electrodynamic Interactions Between Charged Space Systems and the Ionospheric Plasma Environment," Ph.D. Dissertation, Dept. of Aeronautics and Astronautics, Cambridge, MA, June 1995.

[25]Rosenberg, D., and Wehner, G. K., "Sputtering Yields for Low Energy He+-Kr+-, and Xe+-Ion Bombardment," *Journal of Applied Physics*, Vol. 33, No. 5, 1962, pp. 1842–1845.

[26]Chapman, B., *Glow Discharge Processes*, Wiley, New York, 1980.
[27]Gallimore, A. D., Kim, S. W., King, L. B., Foster, J. E., and Gulczinski F. S., III, "Near and Far-Field Plume Studies of a 1 kW Arcjet," *Journal of Propulsion and Power*, Vol. 12, No. 1, 1996, pp. 105–111.
[28]Marrese, C. M., Haas, J. M., Domonkos, M. T., Gallimore, A. D., Tverdoklebov, S., and Garner, C., "D-100 Performance and Plume Characteristics on Krypton," AIAA paper 96-2969, July 1996.
[29]Oh, D., and Hastings, D., "Axisymmetric PIC-DSMC Simulations of SPT Plumes," Electric Propulsion Conf., Paper 95-160, Sept. 1995.
[30]King, L. B., and Gallimore, A. D., "Ionic and Neutral Particle Transport Property Measurements in the Plume of an SPT-100," AIAA Paper 96-2712, July 1996.
[31]Larson, W. J., and Wertz, J. R., *Space Mission Analysis and Design*, 2nd ed., Microcosm, Torrance, CA, 1992.